

The random-field specific heat critical behavior at high magnetic concentration: $\text{Fe}_{0.93}\text{Zn}_{0.07}\text{F}_2$

Z. Slanič and D. P. Belanger

*Department of Physics, University of California
Santa Cruz, CA 95064, USA*

(October 6, 2018)

The specific heat critical behavior is measured and analyzed for a single crystal of the random-field Ising system $\text{Fe}_{0.93}\text{Zn}_{0.07}\text{F}_2$ using pulsed heat and optical birefringence techniques. This high magnetic concentration sample does not exhibit the severe scattering hysteresis at low temperature seen in lower concentration samples and its behavior is therefore that of an equilibrium random-field Ising model system. The equivalence of the behavior observed with pulsed heat techniques and optical birefringence is established. The critical peak appears to be a symmetric, logarithmic divergence, in disagreement with random-field model computer simulations. The random-field specific heat scaling function is determined.

75.40.-s,75.50.Ee,75.50.Lk

I. INTRODUCTION

It has been known experimentally and theoretically for several years that a phase transition occurs¹ for the three-dimensional ($d = 3$) random field Ising model (RFIM). The first evidence² for the phase transition came from the measurement of $(d(\Delta n)/dT)$, where Δn is the optical linear birefringence and T is the temperature. It has long been held^{3,4} that $d(\Delta n)/dT$ is proportional to the magnetic component of the specific heat in anisotropic antiferromagnets to a high degree of accuracy. This has been shown explicitly⁵ for the pure three dimensional ($d = 3$) antiferromagnets MnF_2 and FeF_2 and for the magnetically dilute system⁶ $\text{Fe}_{0.46}\text{Zn}_{0.54}\text{F}_2$ using optical and pulsed heat techniques. The specific heat critical behavior can be obtained in principle from either technique. In applicable cases, however, the birefringence technique is preferable for two reasons. First, the non-magnetic contribution to $d(\Delta n)/dT$ is insignificant, whereas the non-magnetic phonon background for the pulsed heat technique is often large and difficult to eliminate for the purposes of analyzing the magnetic critical behavior. Second, by aligning the probing laser beam to be perpendicular to the inevitable concentration gradients in dilute crystals, one can greatly minimize the effects of the concentration variations that often mask the true critical behavior⁷. Thus, using the optical technique allows data to be taken much closer to the transition. For measurements in an applied field $H > 0$, the birefringence method works well for measuring magnetic specific heat critical behavior, as should techniques that are sensitive to the uniform magnetization, e.g. magnetometry or optical Faraday rotation. The universal critical exponent α and amplitude ratio A^+/A^- for the specific heat for $H > 0$ can be measured with any one of these techniques as well as with the pulsed heat technique. The only difference is in the field dependence of the amplitudes.

The scaling behavior of the amplitudes for dilute antiferromagnets has been worked out by Kleemann, et al.⁸ by considering leading singularities in derivatives of the free energy for $H > 0$. The magnetic specific heat for small fields near the phase transition has the dependence

$$C^m = h_{RF}^{(2/\phi)(\alpha-\alpha^*)} g(|t_h| h_{RF}^{-2/\phi}) \sim h_{RF}^{(2/\phi)(\alpha-\alpha^*)} |t|^{-\alpha} \quad (1)$$

where $t_h = (T - T_N + bH^2)/T_N$, T_N is the zero field transition temperature, $T_c(H)$ is the transition temperature in the field, b is a mean-field temperature shift coefficient, $t = (T - T_c(H))/T_c(H)$ is the reduced temperature, α^* is the $H = 0$ random-exchange specific heat critical exponent, α is the $H > 0$ random-field exponent, h_{RF} is the random-field strength which is proportional⁹ to the applied field H , and ϕ is the random-exchange to random-field crossover exponent. Note that since our maximum applied field $H = 7$ T is much smaller than the spin-flop field¹⁰ $H_{SF} = 41.9$ T for FeF_2 , the demagnetization field corrections are negligible. Similarly, the uniform magnetization measurements yield the scaling behavior

$$\left(\frac{\partial M}{\partial T}\right)_H \sim h_{RF}^{(2/\phi)(1+\alpha-\alpha^*-\phi/2)} |t|^{-\alpha} \quad (2)$$

and

$$\left(\frac{\partial M}{\partial H}\right)_T \sim h_{RF}^{(2/\phi)(2+\alpha-\alpha^*-\phi)} |t|^{-\alpha} \quad . \quad (3)$$

The Faraday rotation yields the same scaling behavior as the uniform magnetization. $d(\Delta n)/dT$ is expected to yield the scaling behavior of the magnetic specific heat, C^m . The proportionality between C^m and $d(\Delta n)/dT$ is valid in the critical region for very anisotropic antiferromagnets. This is true to a high degree of accuracy¹¹ for $\text{Mn}_x\text{Zn}_{1-x}\text{F}_2$ for all concentrations that show critical behavior. The order of magnitude larger anisotropy of $\text{Fe}_x\text{Zn}_{1-x}\text{F}_2$ ensures even greater accuracy.

The primary motivation for returning to the study of the specific heat critical behavior of dilute anisotropic antiferromagnets is to characterize the universal parameters of the random-field Ising model (RFIM) in a system which shows equilibrium behavior below $T_c(H)$. With a small applied field along the easy axis, dilute anisotropic antiferromagnets are proposed as ideal examples of the RFIM, the same critical behavior universality class as a ferromagnet with an applied random field⁹. Since most computer simulation studies of the critical behavior have been made using the latter model, the relevance of the comparison between the experiments and simulations rests on the universality of the behavior of the two systems. However, the correspondence has been far from obvious in most cases since the experiments have been done using crystals with $x < 0.80$. Low temperature hysteresis in the scattering line shapes and anomalous behavior of the Bragg scattering intensity versus T in these crystals have prevented a comprehensive characterization of the random-field critical behavior, particularly for $T < T_c(H)$. In particular, no long-range order is observed after cooling in a field for $x < 0.80$. Although the applied fields are small enough to ensure proper comparison with theory valid in the small random-field limit, the dramatic role of the numerous vacancies at these concentrations had not been fully appreciated until recently. When the number of vacancies is too large, domains can form with little energy cost since the walls pass predominantly through the vacancies^{12,13}. Studies^{14,15} on the bulk crystal $\text{Fe}_{0.46}\text{Zn}_{0.54}\text{F}_2$ and the epitaxial film $\text{Fe}_{0.52}\text{Zn}_{0.48}\text{F}_2$ have demonstrated this. In contrast, the crystal used in the present experiments, with $x = 0.93$, shows no anomaly in the Bragg scattering intensity and no low temperature hysteresis in the scattering line shapes¹⁶. Unlike the lower concentration samples, long-range order is observed upon cooling in an applied field. This is attributed to the low vacancy density and the corresponding energy cost of domain formation. Only at high magnetic concentration might the Imry-Ma domain arguments¹⁷ be applicable. Hence, the $\text{Fe}_{0.93}\text{Zn}_{0.07}\text{F}_2$ crystal affords us the opportunity to characterize the random-field critical behavior in a system that exhibits equilibrium behavior below the transition. We characterize the specific heat critical behavior of this sample and make comparisons to earlier studies⁶ at lower concentration. The fact that the crossover from REIM to RFIM behavior occurs within the critical region, i.e. for $|t| \ll 0.1$ allows us to also determine the crossover function $g(|t_h|h^{-2/\phi})$ in Eq. 1.

A secondary reason to examine this sample, and in particular to do pulsed specific heat as well as birefringence measurements, is to verify the proportionality of the data obtained from these two techniques since this has been questioned¹⁸ in recent series of letters and review articles proposing the so-called “trompe l’oeil” phenomenological model. The model attempts to explain the anomalous behavior of the Bragg scattering $\text{Fe}_{0.5}\text{Zn}_{0.5}\text{F}_2$ and $\text{Mn}_{0.75}\text{Zn}_{0.25}\text{F}_2$ as a violation of RFIM scaling laws. The model requires that C^m and $d(\Delta n)/dT$ (or dM/dT) exhibit different critical behavior in dilute antiferromagnets once a field is applied and, in fact, to exhibit peaks at different temperatures. We can use the measurements on $\text{Fe}_{0.93}\text{Zn}_{0.07}\text{F}_2$ along with previous ones on $\text{Fe}_{0.46}\text{Zn}_{0.54}\text{F}_2$ to test this proposition. We will examine whether the data are consistent with conventional RFIM scaling theory properties and the formation of domains at low temperature or, rather, with the alternative proposed “trompe l’oeil” phenomenology.

II. EXPERIMENTAL DETAILS

Pure FeF_2 is an excellent Ising system owing to its large anisotropy and dominating second-nearest neighbor interaction¹. Mixed crystals of FeF_2 and ZnF_2 can be grown with high crystalline quality, very small concentration gradients and no indication of chemical clustering. The Ising character is preserved upon dilution. The $\text{Fe}_{0.93}\text{Zn}_{0.07}\text{F}_2$ crystal used in the pulsed heat measurements exhibits a rounding of the transition temperature for $|t| < 2 \times 10^{-3}$ due to the concentration variation determined from room temperature Δn measurements⁷. The birefringence data are rounded only for $|t| < 2 \times 10^{-4}$ since the probing laser is oriented in a direction perpendicular to the gradient.

The boule from which the $\text{Fe}_{0.93}\text{Zn}_{0.07}\text{F}_2$ crystal was cut was grown¹⁹ at the University of California, Santa Barbara. The concentration gradient profile was measured using room temperature birefringence and the 1.345 g sample was cut from the portion of greatest homogeneity. The magnetic concentration was determined from the zero field transition temperature which is linear¹ for $0.4 < x < 1.0$.

For the Δn measurements, two parallel faces were polished parallel to the c-axis. The laser beam ($\lambda = 632.8$ nm) traverses a sample thickness of 3.27 mm. The sample was oriented with its c-axis parallel to H . A 0.5 mm pin-hole

in front of the sample minimizes the effects of concentration gradients and vibrations. The Sénarmont technique is used to measure Δn with a resolution of 2×10^{-9} . A commercially calibrated carbon resistor thermometer was chosen for temperature measurement and control because of its low field dependence and high sensitivity. It was possible to achieve temperature stability better than $50 \mu\text{K}$. The same thermometer was later used in the specific heat measurement and was then also calibrated in field vs. another thermometer, whose field dependence is known (see below).

Three different thermal procedures were employed. For zero-field-cooling (ZFC), the sample is first cooled below $T_c(H)$ with $H = 0$, the field is subsequently raised and the sample is slowly heated through $T_c(H)$ in small temperature steps. Specific heat measurements show that the sample temperature usually stabilizes after about 120 s after the application of the heat pulse. The temperature in the birefringence measurements is typically stabilized at each temperature step for approximately 400 s before a Δn measurement is taken, thereby giving the sample ample time to come to equilibrium. For field-cooling (FC), the field is raised well above $T_c(H)$ and the sample is cooled through $T_c(H)$ as data are taken in the manner described above. For field heating (FH), the sample is first FC and then data are taken while the temperature is increased. The temperature steps in all cases were approximately 0.5 K far away from the transition decreasing to 0.005 K close to $T_c(H)$. Reasonable variations in the rates of heating and cooling and stabilization times had no observable effect on the data.

For the adiabatic heat pulse technique, the sample chamber is mounted onto the cold finger via a narrow copper neck. A thermal shield surrounds the sample chamber and the neck. It is fixed to the cold finger and is therefore at the same temperature as the cold finger, i.e. at the temperature of the nitrogen bath. A heater wire, controlled by the temperature controller, is wrapped tightly around and varnished onto the neck below the mounting point for the thermal shield. Two carbon resistor thermometers are mounted into the neck below the heater but above the sample chamber. It is assumed that the neck below the heater, the two thermometers in the neck and the sample chamber are at the same temperature, controlled by the heater on the neck.

The sample is mounted on a thin sapphire plate using GE7031 varnish along with a small Stablohm 800 wire heater. The heater is connected to a four-wire constant-power supply. An unshielded carbon thermometer is attached with varnish to the sample and is connected using a four-wire technique to a current ratio transformer bridge. An unshielded thermometer was chosen to minimize the thermometer's specific heat contribution. The sample is suspended inside the sample chamber by the 0.0254 mm Cu wires used for the thermometer and heater. Care is taken to ensure that the c-axis of the sample is parallel to H . The wires provide a small heat leak from the sample controlled by the temperature difference, δT , between the sample chamber and the sample. The sample thermometer produces a small amount of heat which is compensated by the controlled heat leak so that, in the absence of the heat pulse, the sample temperature is constant. One thermometer located in the neck above the sample chamber is connected to the same bridge as the sample thermometer and is used to control δT . A second thermometer in the neck is used with a second bridge to determine the absolute temperature of the neck and is commercially calibrated for $H = 0$. This thermometer is the same as the one used in the optical birefringence measurement. A preliminary experiment is performed to calibrate δT versus T for sample temperature stability. The calibration is incorporated into the computer control algorithms so that the balance is automatically preserved over the entire temperature range during the specific heat experiment.

During a ZFC experimental run, the sample temperature is first lowered well below $T_c(H)$. The field is then raised. An equilibrium temperature difference between the sample and the sample chamber is found with a temperature drift of the sample of $50 \mu\text{K}$ per minute or less. The absolute temperature of the sample chamber is measured and a heat pulse is applied. The total heat pulse is controlled by the duration of the $907 \mu\text{W}$ pulse. A typical 18 mJ pulse results in a temperature change of approximately 0.025 K, corresponding to a change of 3×10^{-4} in reduced temperature, t , close to $T_c(H)$. As the temperature increases, δT is kept constant, so the temperature of the sample chamber rises as the sample heats. After the application of the heat pulse, the sample is given 300 s to equilibrate and the temperature of the sample chamber is recorded. δT is then set to the new correct value corresponding to the new temperature. The next heat pulse is then applied.

A FC technique completely equivalent to the one used in birefringence is difficult since it is difficult to extract a known amount of heat from the sample. Instead, for the FC technique, the sample temperature is set to a value well above $T_c(H)$. The sample chamber temperature is then lowered by turning off the sample chamber heater, thereby causing the sample and chamber to slowly cool. After approximately 15 to 20 min, the heater is turned on and the sample chamber temperature is increased. The sample chamber temperature is then measured and δT is adjusted alternately until the sample is equilibrated. A heat pulse is applied to the sample and the change of temperature is measured as described for ZFC. The sample temperature is then lowered again. Using reasonably different-sized cooling steps did not significantly affect the data.

After collecting all the data, the sample is removed from the sample chamber and the thermometer is fixed to the sapphire plate. The specific heat of the thermometer, the sapphire plate, the varnish and the wires is then measured at $H = 0$. This background specific heat is subtracted from all of the specific heat data before further analysis.

To calibrate the thermometer field dependence in the temperature region of the transitions, the temperature of the sample is stabilized near and below where the transition takes place in 7 Tesla. The field is then raised to 3 Tesla and the new resistance of the sample thermometer is measured. The field is then decreased at the same rate as it was increased before. The sample thermometer resistance is measured again. If one assumes that the sample was heated equally during the field decrease and increase, then the resistance measured at 3 Tesla corresponds to the mean value of the initial and final resistance in zero field. The thermometer is therefore calibrated at that temperature for 3 Tesla. The procedure is then repeated for 5 and 7 Tesla. A cubic spline interpolation is used to find the temperature (or resistance) corrections for all the other fields. The whole process is repeated at a temperature near and above the zero field transition. The field corrections for all the temperatures between the two calibrated temperatures is arrived at by the use of linear interpolation between the calibrated temperature points. Since the field corrections are small, this procedure yields sufficient accuracy.

At the end of the experiment, the sample thermometer was mounted onto the sample chamber by GE7031 varnish. The uncalibrated thermometer in the neck and the sample thermometer were then calibrated against the commercially calibrated thermometer in the neck. Afterwards, all the thermometers were also calibrated in field. It was possible to determine field corrections for the two thermometers in the neck, since the behavior of the sample thermometer in the field was known.

It should be noted that the unshielded thermometer shows significant variations in resistance after the temperature is cycled to room temperature and cooled again. If one uses the calibration obtained in the process described in the previous chapter, the birefringence and the specific heat data do not coincide, even in zero field. The two shielded thermometers in the neck, however, behaved very consistently and within the specified tolerances. The sample thermometer was recalibrated after every cycling using the sample's zero field transition temperature, for which there is no ambiguity. The measured resistance was multiplied by the required factor so that the birefringence and the specific heat data zero field transition temperatures agreed. The changes in the resistance vs. temperature curves for the sample thermometers probably come from induced strain in the thermometer when it is cycled to the room temperature.

III. RESULTS AND DISCUSSION

The magnetic specific heat behaviors measured using the birefringence technique with $H = 0, 5$ and 7 T are shown in Fig. 1. In the main figure we show $H = 0$ data and, for $H > 0$, ZFC data. In the inset we show both the ZFC and FC data for $H = 7$ T demonstrating the hysteresis extremely close to $T_c(H)$. The curves in this figure are not fits to the data but simply represent the smoothed behavior of the data. Just as observed at lower concentrations, FC yields a more rounded behavior close to T_c .

Figure 2 shows the magnetic specific heat C^m , obtained from the pulsed heat data C_p by subtracting the nonmagnetic background. We are able to do the background subtraction to a good degree of accuracy by first determining the background at $H = 0$. This is done by comparing the $d(\Delta n)/dT$ and C_p data, assuming the $d(\Delta n)/dT$ nonmagnetic background is negligible and that $d(\Delta n)/dT$ and C^m are proportional at $H = 0$. The excess signal found in the C_p data is then taken to be the nonmagnetic contribution to the specific heat, an otherwise difficult quantity to obtain. Within the accuracy of the measurements, the proportionality between $d(\Delta n)/dT$ and C^m , $A = 9.17 \times 10^{-6}$, is the same as that obtained for pure FeF_2 and $\text{Fe}_{0.46}\text{Zn}_{0.54}\text{F}_2$, i.e. the proportionality is independent of the concentration. Once the nonmagnetic contribution to the specific heat is determined, it is subtracted from all of the specific heat data sets. The ZFC data in the main figure are more rounded than the corresponding $d(\Delta n)/dT$ data shown in Fig. 1, a consequence of the greater variation in the concentration gradient across the sample since the whole crystal is used in the C_p measurement. The solid curves in the main figure are obtained from the ZFC $d(\Delta n)/dT$ data by numerically rounding a cubic spline fit of the data to match the concentration variation in the specific heat sample and then drawing smooth curves through the rounded spline fit. The rounded curves are then transferred to the ZFC data in Fig. 2. No other adjustments are made. The data are clearly well represented by the curves, demonstrating that the difference in the appearance of the ZFC $d(\Delta n)/dT$ and C^m data is attributable entirely to the concentration gradient in the sample. The FC behavior at $H = 7$ T is shown in the inset of Fig. 2. The curves are taken from the $d(\Delta n)/dT$ data in the same manner as described above. The FC curve describes the data well, again showing that the $d(\Delta n)/dT$ and C^m data are clearly proportional, once one properly accounts for the gradient effects. The dotted curve is the one corresponding to the ZFC data and is the same as the solid curve in the main figure. The ZFC data are not shown in the inset simply to preserve clarity, but the agreement with the ZFC curve and data is evident from the main figure. The fact that there is only a small difference between the ZFC and FC C^m behavior, relative to the $d(\Delta n)/dT$ data, is simply a consequence of the concentration variation sampled with the C^m technique. Experiments such as the one¹⁸ performed on $\text{Fe}_{0.5}\text{Zn}_{0.5}\text{F}_2$ which do not exhibit hysteresis most likely suffer from concentration

gradients and should not be taken as evidence that hysteresis is absent. Indeed, the $\text{Fe}_{0.46}\text{Zn}_{0.54}\text{F}_2$ crystal, which is of superb homogeneity with $\delta x < 2 \times 10^{-4}$, clearly shows hysteresis in the specific heat⁶.

We do not show the FH $d(\Delta n)/dT$ data since they behave nearly indistinguishably from the ZFC data. This implies that once the sample is FC to low temperatures, the resulting state must be extremely close to that of the ZFC one.

Since we have clearly established that $d(\Delta n)/dT$ and C^m experiments yield the same critical behavior for all H , we will concentrate on the former, which are less affected by gradients and have less ambiguity associated with the nonmagnetic background. Figure 3 shows $d(\Delta n)/dT$ versus the logarithm of t for $H = 0, 2, 5$ and 7 T. For $H = 0$, the data are consistent with an asymmetric cusp, the expected random-exchange critical behavior. However, directly fitting the data did not give as reliable an exponent as we were able to infer from the scaling behavior to be discussed below. The ZFC critical behavior at $H = 7$ T is quite different. We do not observe significant rounding for the fields and reduced temperatures accessed. For $|t| < 2.5 \times 10^{-3}$, the data for $T > T_c(H)$ and $T < T_c(H)$ lie on the same straight line, indicating a symmetric logarithmic divergence (i.e. $\alpha = 0$). At lower fields the data also exhibit the symmetric logarithmic divergence, but over a smaller range in $|t|$, a consequence of crossover. The logarithmic peak has been observed previously²⁰ using Faraday rotation in $\text{Fe}_{0.47}\text{Zn}_{0.53}\text{F}_2$ in a range of $|t|$ extending to much larger values for comparable applied fields. However, in this case rounding occurs at very small $|t|$, which has been attributed to activated dynamic critical behavior. Such rounding is not observed in $\text{Fe}_{0.97}\text{Zn}_{0.07}\text{F}_2$. This may be a result of using fields too small to observe dynamic rounding for $|t| > 10^{-4}$. Interestingly, the FC data also show the symmetric logarithmic behavior and the same crossover behavior with the only difference being the rounding at very small $|t|$. Hence, it is probable that the symmetric logarithm reflects equilibrium behavior and FC simply superimposes rounding on top of it. The FC rounding is consistent with the incomplete development of long-range order as a result of the activated dynamics and the associated logarithmic relaxations near $T_c(H)$. Since the $x = 0.93$ sample shows no low temperature hysteresis in the scattering line shapes, in contrast to those at lower concentrations, and the specific heat nevertheless shows the same logarithmic divergence, we can conclude that the nonequilibrium behavior observed in the lower concentration samples has little effect on the specific heat critical behavior. This is consistent with the fact that the specific heat involves primarily short range fluctuations, whereas the scattering is sensitive to longer-range correlations, which are more affected by domain formation.

The logarithmic divergence is not in agreement with computer simulation results, though many of the other exponents obtained from scattering experiments are to a reasonable extent in agreement. Rieger²¹ obtains the simulation result $\alpha \approx -0.5$, for example, compared with our $\alpha \approx 0$. Nevertheless, the symmetric logarithm is a feature observed in all experiments accurate enough to probe the critical behavior from $x = 0.46$ to 0.93 .

For the range of field accessible in the present experiments, the crossover from random-exchange to random-field critical behavior in $\text{Fe}_{0.93}\text{Zn}_{0.07}\text{F}_2$ takes place well within the critical region, i.e. for $|t| \ll 0.1$. It is therefore feasible to study the crossover function as in Eq. 1 without influences from crossover to mean-field or any other kind of behavior. Fig. 4 shows all of the ZFC birefringence data properly scaled. The solid curves indicate the $\log_{10} |t|$ asymptotic behavior. The scaled data $h_{RF}^{2\alpha^*/\phi} C^m/R$, however, follow the behavior of the full scaling function over a wide range of the variable $th_{RF}^{-2/\phi}$. The $H = 7$ T data cover the range $|t| < 0.1$, while the other sets of data cover correspondingly smaller ranges in $|t|$. The data sets collapse in a satisfactory way except for the lower field ones close to $T_c(H)$. A simple simulation of the effect of the concentration gradient, however, clearly establishes that near $T_c(H)$ the data should be suppressed, with the effect being more noticeable at low fields and with a rounding roughly following the observed effect. In this scaling, we have assumed $\alpha = 0$. The value of the REIM exponent α^* which yields the best scaling collapse is $\alpha^* = -0.10 \pm 0.02$, in excellent agreement with an earlier estimate $\alpha^* = -0.09 \pm 0.03$ taken from direct analysis²² of the critical behavior in $\text{Fe}_{0.6}\text{Zn}_{0.4}\text{F}_2$. Note that the scaling of $d(\Delta n)/dT$ as predicted for the specific heat clearly supports the equivalence of the data from the optical and pulsed heat techniques within a simple proportionality.

Recently, the local mean-field simulation technique has been used by Raposo and Coutinho-Filho to investigate the concentration dependence of domain formation in the dilute antiferromagnets²³. Preliminary results indicate that domain formation does occur only below a critical concentration, which increases with the application of an external magnetic field. Such studies will help to elucidate the nature of the experiments at low and high magnetic concentration.

The results of this study are not consistent with the interpretation of the anomalous Bragg scattering at low magnetic concentrations which has been proposed¹⁸ in a series of papers by Birgeneau, et al. and called “trompe l’oeil” behavior. Two propositions must necessarily hold true for the “trompe l’oeil” phenomenological model to adequately account for the data. First, the $d(\Delta n)/dT$ data must not exhibit the specific heat behavior. In fact, the peaks of the specific heat for $H > 0$ must not coincide in temperature with the peaks in dM/dT or $d(\Delta n)/dT$, though at $H = 0$ they must. The “trompe l’oeil” experimental reports do argue that the peaks occur at different temperatures, but the temperatures of the data were shifted arbitrarily²⁴. Second, the specific heat must not show the FC/ZFC hysteresis near $T_c(H)$ that is seen in the other measurements. Neither of these points are satisfied by

measurements taken using $\text{Fe}_{0.46}\text{Zn}_{0.54}\text{F}_2$ or $\text{Fe}_{0.93}\text{Zn}_{0.07}\text{F}_2$. Hence, the high resolution, low concentration gradient experiments simply do not support the proposed nonscaling “trompe l’oeil” model.

We have presented a study of the specific heat critical behavior of the RFIM system which establishes that the pulsed specific heat and $d(\Delta n)/dT$ yield the same behavior. We have demonstrated that the RFIM specific heat critical behavior obeys the predicted⁸ scaling behavior. We have shown that the critical behavior of the specific heat consists of an asymptotic, symmetric, logarithmic divergence to a very good approximation, in disagreement with computer simulations²¹ indicating a nondivergent specific heat. A companion study¹⁶ of the scattering in the same crystal complements this study in an effort to provide a comprehensive characterization of the static equilibrium critical behavior of the RFIM.

This work was funded by Department of Energy Grant No. DE-FG03-87ER45324. We thank Ernesto Raposo for interesting discussions.

-
- ¹ For a review, see D. P. Belanger and A. P. Young, *J. Mag. Mag. Mater.* **100**, 272, (1991).
² D.P. Belanger, A. R. King, V. Jaccarino and J. L. Cardy, *Phys. Rev. B* **28**, 2522, (1983).
³ J. Ferré and G. A. Gehring, *Rep. Prog. Phys.* **47**, 513, (1984).
⁴ D. P. Belanger, A. R. King, and V. Jaccarino, *Phys. Rev. B* **29**, 2636, (1984).
⁵ D. P. Belanger, P. Nordblad, A. R. King, V. Jaccarino, L. Lundgren and O. Beckman, *J. Magn. Magn. Mater.* **31-34**, 1095, (1983).
⁶ K. E. Dow and D. P. Belanger, *Phys. Rev. B* **39**, 4418, (1989).
⁷ A. R. King, I. B. Ferreira, V. Jaccarino and D. P. Belanger, *Phys. Rev. B* **37**, 219, (1988); D. P. Belanger, A. R. King, I. B. Ferreira and V. Jaccarino, *Phys. Rev. B* **37**, 226 (1988).
⁸ W. Kleemann, A. R. King and V. Jaccarino, *Phys. Rev. B* **34**, 479 (1986).
⁹ J. L. Cardy, *Phys. Rev. B*, **29**, 505, (1984).
¹⁰ V. Jaccarino, A. R. King, M. Motokawa, T. Sakakibara, and M. Date, *J. Magn. Magn. Mater.* **31-34**, 1117, (1983).
¹¹ C. A. Ramos, A. R. King, and V. Jaccarino, *Phys. Rev. B* **37**, 5483, (1988).
¹² U. Nowak and K. D. Usadel, *Phys. Rev. B* **44**, 7426, (1991); *Phys. Rev. B* **46**, 8329, (1992).
¹³ S.-J. Han and D. P. Belanger, *Phys. Rev. B* **46**, 2926, (1992);
¹⁴ D. P. Belanger, A. R. King, V. Jaccarino, and R. M. Nicklow, *Phys. Rev. Lett.* **59**, 930, (1987).
¹⁵ D. P. Belanger, J. Wang, Z. Slanič, S.-J. Han, R.M. Nicklow, M. Lui, C.A. Ramos, and D. Lederman, *J. Magn. Magn. Mater.* **140-144**, 1549 (1995); *Phys. Rev. B* **54**, 3420 (1995).
¹⁶ Z. Slanič, D. P. Belanger, and J. A. Fernandez-Baca, to be published in the *J. Magn. Magn. Mater.* proceedings of ICM’97.
¹⁷ Y. Imry and S. K. Ma, *Phys. Rev. Lett.* **35**, 1399, (1975).
¹⁸ R. J. Birgeneau, Q. Feng, Q. J. Harris, J. P. Hill, A. P. Ramirez and T. R. Thurston, *Phys. Rev. Lett.* **75**, 1198, (1995); *Phys. Rev. Lett.* **77**, 2342, (1996); Q. Feng, Q. J. Harris, R. J. Birgeneau and J. P. Hill, *Phys. Rev. B* **55**, 370 (1997); J. P. Hill, Q. Feng, Q. J. Harris, R. J. Birgeneau, A. P. Ramirez and A. Cassanho, *Phys. Rev. B* **55**, 356 (1997).
¹⁹ The crystal was grown by N. Nighman and cut by A. R. King in the laboratory of V. Jaccarino at UCSB.
²⁰ P. Pollak, W. Kleemann and D. P. Belanger, *Phys. Rev. B* **38**, 4773 (1988).
²¹ H. Rieger, *Phys. Rev. B* **52**, 6659 (1995); H. Rieger and A. P. Young, *J. Phys. A* **26**, 5279 (1993).
²² R. J. Birgeneau, R. A. Cowley, H. Yoshizawa, D. P. Belanger, A. R. King and V. Jaccarino, *Phys. Rev. B* **27**, 6747 (1983).
²³ E. P. Raposo and M. D. Coutinho-Filho, to be published in *Phys. Rev. B*.
²⁴ D. P. Belanger, W. Kleemann and F. C. Montenegro, *Phys. Rev. Lett.* **77**, (1996).

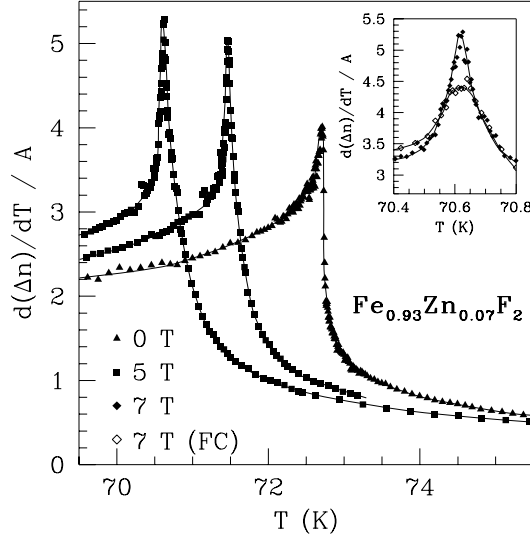


FIG. 1. $d(\Delta n)/dT$ vs. T for $\text{Fe}_{0.93}\text{Zn}_{0.07}\text{F}_2$. $A = 9.17 \times 10^{-6} \text{ K}^{-1}$ is the same proportionality constant found between C_m/R and $d(\Delta n)/dT$ for pure FeF_2 . ZFC data are shown in the main figure. The inset shows the $H = 7 \text{ T}$ FC data as well as the ZFC data. The curves are simply drawn smoothly through the data.

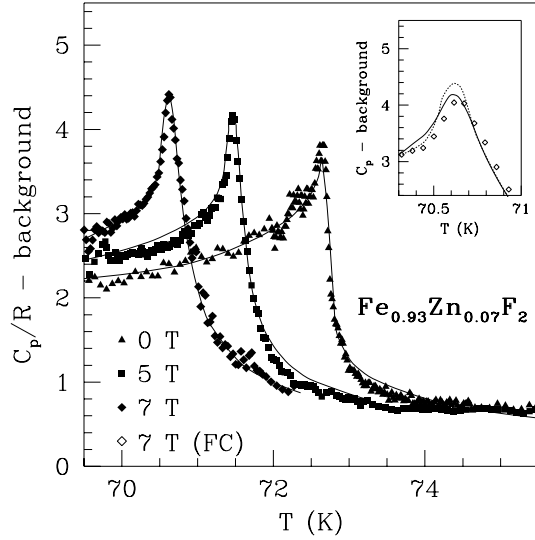


FIG. 2. The magnetic specific heat $C_m = C_p/R - \text{background}$ vs. T for $\text{Fe}_{0.93}\text{Zn}_{0.07}\text{F}_2$. The phonon contribution to the specific heat has been subtracted, as discussed in the text. ZFC data are shown in the main figure. The inset shows the $H = 7 \text{ T}$ FC data. The curves are the same as those in the previous figure except that they are rounded by the larger variation of the concentration gradient, as discussed in the text. The ZFC data are not shown in the inset, for clarity, but the dotted line is the same as the solid ZFC line in the main figure.

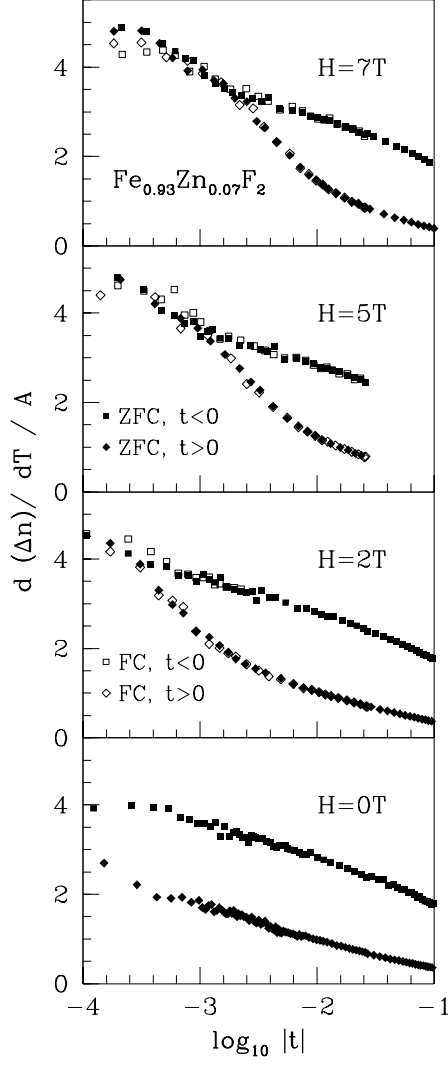


FIG. 3. $d(\Delta n)/AdT =$ vs. $\log_{10} |t|$ for $H = 0, 2, 5$ and 7 T. The solid symbols are for ZFC and the open symbols are for FC. For $H = 0$, the data above and below $T_c(H)$ have distinct amplitudes. In contrast, for $H = 7$ T, the ZFC amplitudes are equal and the data follow an approximate straight line on the semi-log plot for small $|t|$, indicating a symmetric logarithmic divergence. The FC data show significant rounding, but the symmetric logarithmic behavior is still evident. For the smaller fields, the crossover to the symmetric logarithmic behavior occurs much closer to $t = 0$, as expected from scaling.

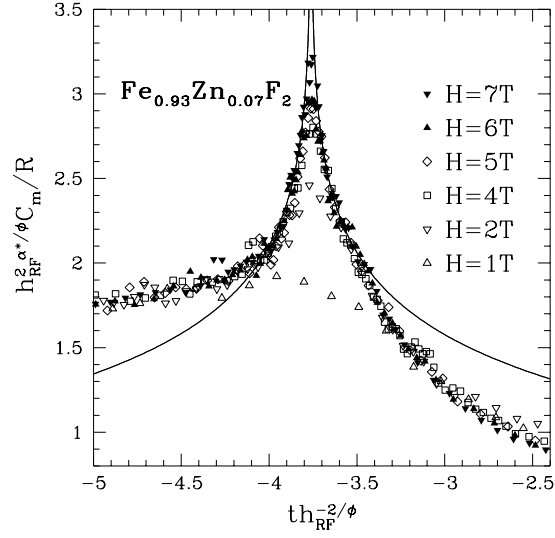


FIG. 4. $h_{RF}^{2\alpha^*/\phi} C_m / R$, using normalized ZFC data obtained with the $d(\Delta n)/dT$ technique, vs. $t h_{RF}^{-2/\phi}$ for $H = 1, 2, 4, 5, 6$ and 7 T. The solid curves represent $h_{RF}^{2\alpha^*/\phi} \ln |t|$, which the data follow in the asymptotic region. The data collapse onto the scaling function in Eq. 1, except for data close to $T_c(H)$, where rounding depresses the peaks. The peak depression is more pronounced at lower fields, as expected, and is consistent with the concentration variation of the sample. For $H = 7$ T, the data span the range $-0.1 < t < 0.1$. For lower fields, the range is appropriately smaller. For this scaling plot we used the $H = 0$ random-exchange exponent $\alpha^* = -0.10$.